Bacterial quorum sensing signal arrests phytoplankton cell division and impacts virus-induced mortality

Scott B. Pollara[a], Jamie W. Becker[a,b], Brook L. Nunn[c], Rene Boiteau[d], Daniel Repeta[e], Miranda C. Mudge[c], Grayton Downing[a], Davis Chase[a], Elizabeth L. Harvey[f*], Kristen E. Whalen[a*]

[a]Department of Biology, Haverford College, Haverford, PA

[b]Present address: Science and Mathematics Department, Alvernia University, Reading, PA

[c]Department of Genome Sciences, University of Washington, Seattle, WA

[d]College of Earth, Ocean, and Atmospheric Sciences, Oregon State University, Corvallis, OR

[e]Marine Chemistry & Geochemistry, Woods Hole Oceanographic Institution, Woods Hole, MA

[f]Department of Biological Sciences, University of New Hampshire, Durham, NH

*Corresponding authors: kwhalen1@haverford.edu; elizabeth.harvey@unh.edu

Running Title: Bacterial signals mediate viral death

Competing Interest Statement: The authors declare no competing interests.

This PDF file includes:

Main Text

Figures 1 to 6

ABSTRACT

Interactions between phytoplankton and heterotrophic bacteria fundamentally shape marine ecosystems by controlling primary production, structuring marine food webs, mediating carbon export, and influencing global climate. Phytoplankton-bacteria interactions are facilitated by secreted compounds; however, linking these chemical signals, their mechanisms of action, and resultant ecological consequences remains a fundamental challenge. The bacterial quorum sensing signal 2-heptyl-4-quinolone (HHQ), induces immediate, yet reversible, cellular stasis (no cell division nor mortality) in the coccolithophore, *Emiliania huxleyi*, however, the mechanism responsible remains unknown. Using transcriptomic and proteomic approaches in combination with diagnostic biochemical and fluorescent cell-based assays, we show that HHQ exposure leads to a prolonged S-phase arrest in phytoplankton coincident with the accumulation of DNA damage and lack of repair despite the induction of the DNA damage response (DDR). While this effect is reversible, HHQ-exposed phytoplankton were also protected from viral mortality, ascribing a new role of quorum sensing signals in regulating multi-trophic interactions. Furthermore, our data demonstrate *in situ* measurements of HHQ coincide with areas of enhanced micro- and nanoplankton biomass. Our results suggest bacterial communication signals as emerging players that may be one of the contributing factors that help structure complex microbial communities throughout the ocean.

IMPORTANCE

Bacteria and phytoplankton form close associations in the ocean that are driven by the exchange of chemical compounds. The bacterial signal 2-heptyl-4-quinolone (HHQ), slows phytoplankton growth, however, the mechanism responsible remains unknown. Here, we show that HHQ exposure leads to the accumulation of DNA damage in phytoplankton and prevents its repair.

While this effect is reversible, HHQ-exposed phytoplankton are also relieved of viral mortality, elevating the ecological consequences of this complex interaction. Further results indicate HHQ may target phytoplankton proteins involved in nucleotide biosynthesis and DNA repair, both of which are crucial targets for viral success. Our results support microbial cues as emerging players in marine ecosystems, providing a new mechanistic framework for how bacterial communication signals mediate interspecies and interkingdom behaviors.

INTRODUCTION

Interactions between marine phytoplankton and bacteria have been shown to fundamentally shape marine ecosystems, particularly by mediating biogeochemical cycling, regulating productivity, and trophic structure [1-3]. Bacteria-phytoplankton interactions are complex, often being species-specific [4] or temporally ephemeral [5] and can span the spectrum from antagonistic to beneficial [6, 7]. Increasingly, it is clear that these intricate inter-kingdom interactions are facilitated by excreted chemical compounds that mediate a suite of processes such as nutrient transfer, primary production, and shifts in community composition. Linking chemical compound identity with a mechanism of action and ecological consequences will strengthen our understanding into how these fundamental and multifaceted interactions govern marine ecosystem function.

First discovered in marine systems four decades ago [8], quorum sensing (QS) is a form of microbial cell-cell communication through which marine bacteria use diffusible chemical signals to facilitate coordinated and cooperative biogeochemically important behaviors [9]. Recent work, finds alkylquinolone-based QS signals can modulate interspecies behavior, suggesting that these molecules may influence cellular communication at the interkingdom level

[10]. In particular, the alkylquinolone QS signal 2-heptyl-4-quinolone (HHQ) functions as a messenger molecule, able to modulate bacterial virulence behavior, facilitating the emergence of the pathogen *Pseudomonas aeruginosa* within polymicrobial communities [11, 12]. Trafficking of hydrophobic alkylquinolones, including HHQ, is aided by the release of outer-membrane vesicles containing micromolar concentrations of alkylquinolones that are produced by *P. aeruginosa* and serve as signal delivery vehicles to neighboring recipient cells [13]. Purified outer-membrane vesicles isolated from *P. aeruginosa* have also been shown to possess significant antimicrobial activity, inhibiting the growth of adjacent Gram-positive bacteria [13]. Additionally, HHQ has also been implicated in antagonizing fungal biofilm formation [12], downregulating eukaryotic host immune response via suppression of a key transcription factor, NF-κB [10], and activating receptors found to play a role in innate immune signaling in airway epithelia [14]. These findings support the influence of alkylquinolones in mediating host-microbe interactions.

Recently, HHQ was isolated from marine gamma-proteobacteria (*Pseudomonas* sp. and *Pseudoalteromonas* sp.) and was observed to cause significant shifts in both natural phytoplankton and microbial communities [15], including species-specific static phytoplankton growth (no growth or mortality) at nanomolar concentrations [16]. Static growth in phytoplankton has been observed previously, in relation to both bacterial exudates [17, 18] and nutrient stress [19-22]. However, the underlying molecular mechanism(s) by which HHQ influences phytoplankton fitness and the outcomes of ecological interactions remain unknown. For example, host physiology has been demonstrated to be an integral factor in the success of viral infection of phytoplankton, with infection success and burst size influenced by host

condition [23]. However, the role that HHQ plays in mediating microbial interactions beyond phytoplankton growth alterations has yet to be investigated.

To better understand how HHQ alters molecular function and ecological interactions in marine microbes, ultrastructural observations and diagnostic biochemical assays were integrated with transcriptomic and proteomic studies to link the persistent but reversible physiological impact of nanomolar concentrations of HHQ on a model marine phytoplankton, *Emiliania huxleyi*. Further, we examined if HHQ could disrupt viral-induced mortality in *E. huxleyi*, thereby ascribing a new role for bacterial quorum sensing signals. *E. huxleyi* plays a central role in mediating ocean carbon [24] and sulfur [25] cycling, thus, the results presented here emphasize the importance of considering the ecological consequences of chemically-mediated bacteria-phytoplankton interactions on global primary production and biogeochemical cycles.

RESULTS AND DISCUSION

Response to HHQ exposure. Following 96 h of exposure to 100 ng ml^{-1} of HHQ, batch cultures of axenic *E. huxleyi* (CCMP 2090) exhibited cellular stasis (no cell division nor mortality) concomitant with a significant increase in forward scatter, red fluorescence, and side scatter, proxies for cell size, chlorophyll content, and cell granularity, respectively (repeated analysis of variance (ANOVAR), p-value < 0.01 for all comparisons;**Fig. 1**). Photosynthetic efficiency (Fv/Fm) did not change in response to long-term HHQ exposure (ANOVAR). Additionally, after only 24 h of HHQ exposure, phytoplankton cells were observed to have enlarged chloroplasts with distended thylakoid membranes containing numerous intra-organelle vesicles, abundant cytoplasmic vesicles/vacuoles, homogenous nuclei staining lacking defined euchromatin/heterochromatin regions with disintegrated nuclear envelops, and osmium-rich

puncta within and adjacent to the chloroplasts likely indicating enhanced lipid storage (**Fig. S1**). To examine if the physiological effects induced by HHQ exposure were reversible, 96 h-exposed HHQ cultures were diluted roughly ~80 fold with f/2 -Si [26] to a final concentration of 1.25 ng ml^{-1} HHQ, a concentration demonstrated to not influence *E. huxleyi* growth. Cells previously exposed to HHQ showed recovery mirroring paired vehicle control cultures (ANOVAR, **Fig. S2**). Taken together, HHQ-treated *E. huxleyi* cells appear to mirror previous studies in which cellular arrest has been observed in phytoplankton in response to bacterially-derived chemical exposure [17, 18, 27-29], as well as nutrient limitation [20-22]. In order to elucidate if the observed cellular stasis is mechanistically similar to previously those observed in the literature, we conducted cell cycle, transcriptomic, and proteomic analysis of HHQ exposed *E. huxleyi*.

Evidence for S-phase arrest. The DNA content of *E. huxleyi* cells following HHQ exposure was tracked for 96 h via flow cytometry, and cells treated with HHQ ceased a typical diurnal cell cycle progression within 24 h of HHQ addition (**Fig. 2**). Over 96 h, the proportion of HHQ-exposed cells in both G1 and G2 phase were shown to steadily decrease, whereas the proportion of cells in S-phase significantly increased (ANOVAR, $p > 0.01$; **Fig. 2c - e**). Additionally, HHQ-exposed cells found in G1 phase demonstrated significantly higher DNA content per cell compared to their paired vehicle controls (Welch's approximate t-test, *p*-value < 0.05; **Fig. 2f**). These results suggest HHQ-exposed cells are attempting to duplicate their genome but stalling in early S-phase.

Whole-cell transcriptomic and proteomic analyses were performed on *E. huxleyi* cells exposed to 1 ng ml^{-1} (low), 10 ng ml^{-1} (medium), and 100 ng ml^{-1} (high) HHQ concentrations, with samples taken at 24 h (transcripts) and 72 h (transcripts and proteins) (**Fig. S3**). *E. huxleyi* cultures demonstrated unique transcriptomic and proteomic profiles in response to each HHQ

concentration, with the greatest numbers of differentially expressed genes found in higher HHQ treatments, when compared to the DMSO vehicle control (**Fig. S3 a, b; Table 1**). After 24 h of HHQ exposure, 39.8% of transcripts in high HHQ samples were differentially expressed relative to DMSO vehicle controls (Wald test, q-value < 0.05; **Table 1**).Similarly, after 72 h of exposure, replicate high HHQ samples continued to appear distinct from the DMSO vehicle control samples (**Fig. S3a,b**), with 37.6% of transcripts (Wald test, q-value < 0.05) and 15.9% of proteins (Welch's approximate t-test, q-value < 0.05) significantly changing in relative abundance and abundance, respectively (**Table 1**). When examined together, a total of 665 genes and corresponding proteins were found to be significantly changing in abundance at 72 h under high HHQ treatment relative to the vehicle control (**Fig. 3,** see **Supplemental Data File 1** at https://doi.org/10.6084/m9.figshare.14414285.v1**)**. In general, processes associated with DNA replication and repair, aerobic respiration, and protein catabolism yielded higher relative transcript and protein abundances under high HHQ treatment, while photosynthetic components/processes were detected at lower relative transcript and protein abundances (**Fig. 3a**, see **Supplemental Data File 1** at https://doi.org/10.6084/m9.figshare.14414285.v1). Far fewer genes and proteins were found to be differentially expressed in the low and medium HHQ treatments (**Table 1**), which is likely related to the observed recovery in cell growth in these treatments (**Fig. S3c**). The growth of cells exposed to low HHQ concentrations was nearly identical to the DMSO control throughout the experiment. By 72 h, no genes or proteins in the low treatment were differentially expressed compared to the control. While the medium HHQ treatment demonstrated some growth inhibition over the first 24 h, by 72 h the population had largely recovered (**Fig. S3c**). For cell populations exposed to medium HHQ concentrations at 24 h, transcripts relating to cell cycle progression, cytoskeletal regulation, and mitosis demonstrated

161 increased relative abundances compared to the control (see **Supplemental Data File 1** at
162 https://doi.org/10.6084/m9.figshare.14414285.v1). By 72 h, there was no clear trend observed in
163 functions relating to differentially expressed transcripts in the medium HHQ samples. For
164 purposes of elucidating the molecular target(s) of HHQ, we therefore focused our efforts on the
165 analysis of the high HHQ transcriptomic and proteomic data.

166 Indeed, at the physiological level, the response of *E. huxleyi* to HHQ parallels phosphorus
167 (P) limitation in phytoplankton (i.e. S/G2 phase arrest, decreased growth rate, and increases in
168 chlorophyll content, forward scatter, and side scatter) [19-21, 30]. However, the canonical
169 response in P-limited cells of upregulation of both alkaline phosphatase and phosphodiesterases
170 [31-33] was not observed in cells exposed to HHQ. Nor do we see significant induction of acid
171 phosphatases, pyrophosphatase, phosphorus transporters, or ATP-sulfurylase enzymes known to
172 be induced following P-limitation in HHQ exposed cells, indicating the lack of phosphorus stress
173 (see **Supplemental Data File 1** at https://doi.org/10.6084/m9.figshare.14414285.v1). Therefore,
174 while the pattern of cell cycle arrest is similar between HHQ-treated *E. huxleyi* and nutrient
175 limitation, the underlying mechanisms are distinct.

176 In phytoplankton, cellular arrest is often accompanied by induction of autocatalytic or
177 programmed cell death (PCD) responses such as increased reactive oxygen production or
178 caspase-like activity [34], and previous findings in mammalian cells indicate that HHQ has the
179 ability to activate PCD pathways [35]. However, no evidence of PCD/apoptosis was observed in
180 HHQ exposed *E. huxleyi* cells using a series of diagnostic fluorescent assays (i.e. membrane
181 permeabilization, caspase activity, reactive oxygen species (ROS), and nitrous oxide (NO)
182 production) (**Fig. S4**). Additionally, no transcripts or proteins associated with PCD increased in
183 abundance with exposure to HHQ (see **Supplemental Data File 1** at

https://doi.org/10.6084/m9.figshare.14414285.v1). The lack of PCD induction in HHQ-exposed cells may stem from *E. huxleyi*'s arrest in early S-phase (**Fig. 2d**), as cellular arrest during S-phase does not induce apoptotic pathways, but rather curtails DNA replication thereby dramatically extending the cell cycle [36]. The transcriptomic profile of HHQ-exposed cells demonstrates an increased relative abundance of canonical transcripts facilitating the G1/S transition including cell division control protein 6 (CDC6), origin recognition complex subunit 1 (ORC1), and cyclins A, B, E, and K (**Fig. 3b**). Moreover, significant increases in relative transcript abundances of DNA replication fork machinery (i.e., DNA polymerases α, ε, and δ, DNA primase, replication protein A, topoisomerases (TOPO), the minichromosomal maintenance complex, proliferating cell nuclear antigen, and replication factor C), (**Fig. 3c**) at 72 h post HHQ exposure, suggests an intent to replicate DNA, a hallmark of S-phase [37]. Yet, despite this observed induction of DNA replication machinery, DNA synthesis was severely curtailed following HHQ exposure (**Fig. 2**), suggesting that HHQ exposure interferes with the ability of *E. huxleyi* cells to correctly complete the DNA replication process.

Disruption of DNA replication induces DNA damage response (DDR) pathways, activating effector kinases such as Chk1 and Chk2 necessary for halting DNA synthesis and induction of cell cycle arrest to allow time for repair [38]. We observed transcripts for Chk1 and Chk2 to be differentially expressed under HHQ treatment (**Fig. 3B**). Further, a significant decrease in relative histone transcript and protein abundance, a hallmark of DNA synthesis disruption, was observed (see **Supplemental Data File 1** at https://doi.org/10.6084/m9.figshare.14414285.v1) following HHQ exposure. As DNA replication and histone production are coupled, cells experiencing DNA replication stress will remove histone transcripts [39].[38]

Possible protein targets of HHQ. During S-phase, a cell must tightly regulate the availability of nucleotides to ensure faithful DNA replication [40]. Therefore S-phase cells rely on *de novo* nucleotide synthesis pathways to produce enough materials for complete genome replication [41]. Several transcripts and proteins involved in *de novo* purine (amidophosphoribosyltransferase, trifunctional purine biosynthetic protein adenosine-3, phosphoribosylformylglycinamidine synthase, bifunctional purine biosynthesis protein, adenylsuccinate synthase, IMP dehydrogenase, and GMP synthase) and pyrimidine (carbamoyl phosphate synthase II, aspartatecarbamoyl transferase, and CTP synthases) nucleotide synthesis increased in abundance with HHQ exposure (see **Supplemental Data File 1** at https://doi.org/10.6084/m9.figshare.14414285.v1). Increased nucleotide synthesis may indicate the need to produce the necessary materials to replenish nucleotide pools during replication. However, only partial replication of the *E. huxleyi* genome following HHQ exposure was observed (**Fig. 2**), suggesting HHQ may disrupt nucleotide production thereby limiting nucleotide availability.

Select alkylquinolones are known to inhibit a key rate-limiting enzyme directly involved in pyrimidine synthesis, dihydroorotate dehydrogenase (DHODH) [42]. DHODH inhibition in eukaryotes may induce an intra-S-phase arrest due to severely diminished cellular nucleotide pools that can disrupt DNA replication, stall replication forks, and increase the frequency of genomic DNA lesions, including strand breaks, during S-phase [43, 44]. Indeed, after 46 h of HHQ exposure, a significant increase in DNA strand breaks was observed in culture (Welch's approximate t-test, $p = 0.032$; **Fig. 4a**), and not observed when HHQ was directly exposed to genomic *E. huxleyi* or Lambda DNA (**Fig. S5**). This indicates that DNA strand breaks are not caused directly by HHQ, but indirectly through other mechanisms. It has been previously

observed that following the induction of DNA damage during S-phase, cells will enter an intra-S phase arrest that drastically slows the rate of DNA replication to allow the DNA damage response (DDR) to resolve any DNA lesions [36]. With the exception of preliminary work in *Chlamydomonas reinhardtii* and dinoflagellates, the DDR response has not been well characterized in phytoplankton [45, 46]. Of the 57 mammalian DDR protein homologs in the *E. huxleyi* genome (e-value $\leq 10^{-20}$), 41 were significantly differentially expressed (at either the transcript and/or protein level), of which 37 increased in relative abundance at 72 h under high HHQ exposure (**Fig. 3c**), indicating the cell is attempting to repair DNA lesions. However, DNA damage induced by the inhibition of DHODH is known to activate apoptotic pathways through the hyperactivation of the DDR [47]. No apoptotic pathway activation was observed with HHQ exposure, suggesting the DDR response itself may also be impacted by HHQ.

A master regulator of the DDR involved in chromatin remodeling, nucleolar structure, and genome stability is poly(ADP-ribose) polymerase (PARP) [48]. PARP binds to sites of DNA damage and stalls replication forks, producing negatively charged ADP-ribose polymer scaffolds that attract repair proteins [49]. PARP homologs in *E. huxleyi* were found to increase in both relative transcript abundance and protein abundance under HHQ treatment (**Fig. 3c**). Under high levels of DNA damage or if repair mechanisms are compromised, PARP can become overactivated and deplete cellular NAD^+ and ATP pools, thereby initiating apoptotic pathways [50]. However, no apoptotic activity was observed in *E. huxleyi* cells following HHQ exposure (**Fig. S4**), indicating HHQ may inhibit PARP activity. Indeed, HHQ was found to significantly inhibit human PARP activity (Welch's approximate t-test, $p = 0.0002$; **Fig. 4b**), while a closely related alkylquinolone, 2-heptyl-3-hydroxy-4(1H)-quinolone (PQS), did not possess PARP inhibitory activity, nor did it impact *E. huxleyi* growth (**Fig. 4b and Fig. S6a**). Interestingly, the

genomes of phytoplankton species unaffected by HHQ [16] did not reveal the presence of any PARP homologs, further implicating PARPs in the response of phytoplankton to HHQ.

Inhibition of PARP activity in the presence of DNA damage drastically reduces the effectiveness of the DDR response and is known to induce cellular arrest in the S-phase [51]. Together, our observations of prolonged S-phase arrest (**Fig. 2**), the upregulation of the DDR response in HHQ-exposed cultures (**Fig. 3c**), the conserved nature of the mammalian and *E. huxleyi* PARP catalytic site (**Fig. S6 b-d**), and the chemical structural similarities of HHQ to known inhibitors of both PARP and DHODH with core benzimidazole moieties [52], collectively suggest that HHQ may function simultaneously to inhibit both PARP and DHODH activity in *E. huxleyi*. Additional experiments using *E. huxleyi* enzymes are needed to fully characterize whether PARP and DHODH are molecular targets of HHQ.

HHQ impacts on energy production. To facilitate DNA synthesis and repair, the cell requires large ATP pools [53]. In HHQ exposed cells, the increased relative transcript abundance of enzymes in the tricarboxylic acid (TCA) cycle (i.e., isocitrate dehydrogenase, α-ketoglutarate dehydrogenase, succinate dehydrogenase, fumarase, and malate dehydrogenase) (see **Supplemental Data File 1** at https://doi.org/10.6084/m9.figshare.14414285.v1) may signal the overproduction of reducing equivalents for ATP production via oxidative phosphorylation. Additionally, the increase in relative transcript abundance of the metabolic efficiency controllers, sirtuin-like deacetylases[54], observed following HHQ treatment (see **Supplemental Data File** 1 at https://doi.org/10.6084/m9.figshare.14414285.v1) may be a direct result of PARP inhibition.Sirtuins compete with PARPs for NAD^+ and expression of deacetylases is dependent on NAD^+ availability [55]. PARP inhibition is known to drastically increase cellular NAD^+ pools, thereby promoting sirtuin expression and activity [56]. Increased sirtuin activity in HHQ

exposed cells may also explain the increase in the relative transcript abundance of manganese superoxide dismutase (Mn-SOD) (see **Supplemental Data File 1** at https://doi.org/10.6084/m9.figshare.14414285.v1), an antioxidant enzyme that protects the cell from ROS induced damage, as sirtuins are known to induce the production of Mn-SOD proteins [57]. Finally, increased relative transcript abundance of the tryptophan-mediated *de novo* NAD^+ synthesis pathway was also observed, potentially in an attempt to increase NAD^+ availability (see **Supplemental Data File 1** at https://doi.org/10.6084/m9.figshare.14414285.v1). Taken together, these results suggest that HHQ exposure promotes increased energy production in *E. huxleyi*, which can fuel various cellular biosynthesis and repair pathways while staving off the induction of PCD.

Increased cellular demand for ATP would necessitate the induction of glycolytic enzymes. However, following HHQ treatment, there was a significant decrease in the relative transcript abundance of hexokinase (see **Supplemental Data File 1** at https://doi.org/10.6084/m9.figshare.14414285.v1), the first step in glycolysis, consistent with previous work demonstrating alkylquinolones suppress induction of this glycolytic enzyme through the direct targeting of the transcription factor hypoxia-inducible factor 1 (HIF-1) protein degradation via proteasomal pathways [58]. Furthermore, we observed a shift to the Entner-Doudoroff glycolytic pathway in HHQ treated cells (see **Supplemental Data File 1** at https://doi.org/10.6084/m9.figshare.14414285.v1), which can conserve amino acid resources due to a lower protein demand in comparison to other pathways [59]. Moreover, we observed increases in the relative transcript abundances leading to the production of aspartate (i.e., TCA cycle, the aspartate-arginosuccinate shunt, glutamic oxaloacetic transaminase (GOT), and C4-like photosynthesis) in parallel with a decrease in transcripts for aspartate utilization pathways,

with the exception of nucleotide synthesis (see **Supplemental Data File 1** at https://doi.org/10.6084/m9.figshare.14414285.v1). Aspartate is known to rescue cells from S-phase arrest by fueling *de novo* nucleotide synthesis [60].

HHQ impacts on photosynthesis and redox. HHQ-induced cell cycle arrest in *E. huxleyi* did not significantly alter photosynthetic energy conversion efficiency, however, the majority of light-harvesting complexes and transcripts of the Calvin cycle decreased in relative abundance under HHQ exposure (**Fig. 3a**). These findings parallel those described for the diatom *Phaeodactylum tricornutum* undergoing chemically-mediated cell cycle arrest [61]. In plants, the coordinated down-regulation of transcripts involved in photosynthesis, electron transport, and the Calvin cycle is thought to allow for the reallocation of resources towards defense against bacterial and viral pathogens [62]. However, a decrease in transcript abundance does not always correlate with a loss of protein function, as photosynthetic proteins have a long functional half-life in the cell with the exception of ferredoxin (Fd) and ferredoxin NADP+ oxidoreductase (FNR), both of which are involved in maintaining cellular redox state following pathogen infection [62]. Together, both ferredoxin and the isofunctional flavodoxin (Fld) participate in electron shuttling, preventing electron misrouting that can lead to ROS accumulation and restoring chloroplast redox homeostasis under environmental stress [63]. Indeed, the genes and proteins with the most significant differential expression levels under HHQ exposure in *E. huxleyi* were Fd (58-fold increase in transcript and 3-fold increase in protein), FNR (85-fold increase in transcript), and Fld (38-fold increase in transcript and 186-fold increase in protein) (**Fig. 3a,** see **Supplemental Data File 1** at https://doi.org/10.6084/m9.figshare.14414285.v1), which may explain the observed lack of ROS production (**Fig. S4**). Additional reduction systems including FAD/NAD(P) oxidoreductases, ferredoxin nitrite reductase (Fd-NR), and glutathione

reductase (GR) in HHQ-treated *E. huxleyi* were also significantly induced which could ameliorate NADPH build-up (see **Supplemental Data File 1** at https://doi.org/10.6084/m9.figshare.14414285.v1). Moreover, increased relative expression of vitamin B6 (VitB6) transcripts following HHQ treatment could protect against oxidative stress in chloroplasts [64], while increased relative expression of transcripts encoding proline oxidase (POX), pyrroline-5-carboxylate reductase (P5CR), and manganese superoxide dismutase (Mn-SOD) could explain the lack of mitochondrial ROS toxicity (**Fig. S4,** see **Supplemental Data File 1** at https://doi.org/10.6084/m9.figshare.14414285.v1). Together, these results suggest that HHQ exposed *E. huxleyi* uniformly decreased the relative abundance of photosynthetic gene transcripts in support of a coordinated induction of defense responses aimed at maintaining cellular redox homeostasis without debilitating photosynthetic capacity.

Consequences of HHQ-induced cellular stasis. Given that viral replication requires hijacking of host-replication machinery and HHQ exposure inhibited DNA replication and repair in *E. huxleyi*, the impact of HHQ on host-virus dynamics was investigated. When *E. huxleyi* cells were exposed to HHQ and *E. huxleyi* virus (EhV) strain 207 concurrently, virus-induced cellular death was significantly reduced (ANOVAR, p-value < 0.0001; **Fig. 5a**). This outcome was observed regardless of whether viruses were added simultaneously with HHQ (**Fig. 5a**) or 72 h post HHQ treatment (**Fig. 5b**). However, if HHQ addition was delayed even by 24 h, viral-induced mortality occurred in *E. huxleyi* (**Fig. 5c**). These results indicate the possibility that HHQ exposure early on in viral infection critically impacts the effectiveness of the virus. There are numerous mechanisms by which HHQ may inhibitvirus-induced mortality of *E. huxleyi* (**Fig. 6**). For example, HHQ may impact the entry of the virus into the cell. Significant morphological restructuring occurred following 24 h HHQ exposure, which may prevent viral recognition,

attachment, and/or endocytosis. Previous work has demonstrated that within 24 h of *E. huxleyi* viral infection, the virus requires the induction of host DNA replication machinery [65]. Thus, HHQ may either inhibit the virus' ability to manipulate DNA replication or acquire necessary nucleotides for transcription, thereby stalling infection success. HHQ may also stall the induction of ROS production, which has been demonstrated previously to be necessary for successful *E. huxleyi* viral infection [66]. In the transcriptomic and proteomic data presented here, significant upregulation of a variety of antioxidants, including Fd, FNR, Fld, Fd-NR, GR, Mn-SOD, POX, and VitB6, may counter act viral-induced remodeling of the host antioxidant network essential for viral replication. Likewise, expression and activation of caspase and metacaspase proteases during infection is critical for enabling virus-induced lysis in *E. huxleyi* [67]. However, these proteases were not upregulated, and did not show activity in HHQ-exposed cells (**Fig. S4,** see **Supplemental Data File 1** at https://doi.org/10.6084/m9.figshare.14414285.v1), further suggesting that HHQ exposure may disrupt these critical processes in viral infection. Attenuation of viral mortality would theoretically permit increased survival of phytoplankton and allow for bacteria to continue to take advantage of coordinated nutrient exchange, common between bacteria and phytoplankton [68]. Thus, the impacts of HHQ exposure on phytoplankton may have ecological consequences beyond shifts in algal physiology, to impacts on large scale biogeochemical cycles.

Summary. Our laboratory findings demonstrate that a quorum sensing signal produced by a marine bacterium significantly, but reversibly, leads to DNA lesions and cell cycle arrest in a eukaryotic phytoplankter, which can influence interkingdom viral-host interactions. In the eastern tropical South Pacific > 1 ng L^{-1} surface concentrations of HHQ were found to correlate with areas of enhanced phytoplankton biomass (**Fig. S7**). These low concentrations of HHQ in

bulk seawater are not surprising, as N-acyl homoserine lactones [69], vitamins [70], and other highly labile, trafficked compounds fundamental to growth and signaling are often found in low concentrations in bulk seawater. We anticipate the primary abiotic sink for HHQ will be photooxidation by sunlight, however the rate of photooxidation in seawater will strongly depend on a myriad of factors (e.g. depth, daylength, DOM concentration, etc). Previous work on the half-life of quinoline, the parent compound of HHQ, varied between 8-53 days using solar simulations [71]. Futhermore, these measured bulk concentrations likely do not represent the effective concentration a marine microbial cell would experience in the phycosphere [72].

Previous work has demonstrated that HHQ can significantly alter natural microbial community composition and growth rates [15], and here we find detectable *in situ* HHQ concentrations correlated with enhanced phytoplankton biomass. Together, these findings suggest that alkylquinolone signaling may play a significant role in structuring complex microbial communities, ultimately, influencing primary production and biogeochemical cycles. In addition, our findings highlight the functional duality of bacteria cues that serve both as diffusive messengers used as a communication tool in microbial communities, but also as chemical mediators of marine microbial interactions.

MATERIALS AND METHODS

General Cultivation Conditions

For all experiments axenic *Emiliania huxleyi* (CCMP2090, non-lith forming)from the National Center for Marine Algae and Microbiota, East Boothbay, Maine) was grown in natural seawater-based f/2 medium without silica [26]. Cultures were maintained on a 14:10 h light (80 ± 5 μmol photons m^{-2} s^{-1}):dark cycle at 18 ^{o}C, and salinity of 35. These conditions will be

391 referred to hereafter as general culturing conditions. Strain purity was confirmed using f/2 MM
392 and f/2 MB purity test broths and visually confirmed by epifluorescence microscopy [73].
393 Cultures (20 ml) were transferred weekly to maintain exponentially growing cultures.
394 Phytoplankton cells were enumerated by hemocytometer or using a flow cytometer
395 (Guava, Millipore). Via the flow cytometer, cell abundance was determined by using species-
396 specific settings including their forward scatter, side scatter, and red fluorescence (695/50 nm)
397 emission characteristics for evaluating chlorophyll intensity. All samples were run at 0.24 µl s^{-1}
398 for 3 min, either live or fixed with glutaraldehyde (0.5% final concentration). A correction factor
399 was applied to fixed cell abundances to account for cell loss due to preservation.
400
401 **Growth Experiments**
402 The HHQ concentration resulting in 50% growth inhibition (IC_{50}) was determined using
403 triplicate, 2 - 20 ml cultures of *E. huxleyi* (~100,000 cells ml^{-1}) exposed to HHQ (between 0.25 –
404 512 ng ml^{-1}), PQS (0.5 – 530 µg ml^{-1}), or vehicle control (0.1% DMSO) for 72 h. Growth rates
405 were calculated using an exponential growth equation and were plotted against HHQ
406 concentration to determine IC_{50} at 72 h post exposure as described previously [16].
407 Concentrations of DMSO below 0.5% v/v have no impact on axenic *E. huxleyi* growth. DMSO
408 was used as the solvent vehicle for HHQ and PQS.
409 To examine the impacts of HHQ, triplicate flasks of 30 ml cultures of *E. huxleyi* (~
410 50,000 cells ml^{-1}) were exposed to either 1 or 100 ng ml^{-1} HHQ, or a vehicle (0.1% DMSO)
411 control. The experiment was sampled daily for 96 h to monitor *E. huxleyi* abundance, forward
412 scatter, side scatter, red fluorescence (695/50 nm), and photosynthetic efficiency (Fv/Fm). Fv/Fm
413 was measured using a Fluorescence Induction and Relaxation (FIRe) system (Satlantic). Samples

were dark adapted for 30 min, and photosystem II kinetics were measured from the average of 10 iterations of an 80 µs single turnover event and 1000 ms of weak modulated light.

To measure recovery, after 96 h of HHQ exposure, triplicate 2 ml aliquots of HHQ-exposed culture was transferred into 198 ml of fresh media, effectively diluting HHQ to 1 ng ml^{-1}. The same dilution was made with the vehicle control treatment, and the experiment was sampled daily for *E. huxleyi* growth rate, forward scatter, side scatter, and red fluorescence (695/50 nm).

To investigate viral infection dynamics, triplicate 50 ml cultures were prepared for the following treatments: *E. huxleyi* (~ 40,000 cells ml^{-1}) + vehicle control (0.1% DMSO), *E. huxleyi* + EhV 207 (3.2 x 10^6 EhV ml^{-1}), *E. huxleyi* + HHQ (100 ng ml^{-1}), *E. huxleyi* + HHQ + EhV 207. The MOI = 80, to ensure successful viral infection potential. Samples were taken daily to monitor *E. huxleyi* abundance.

For all growth experiments, excluding the IC_{50} calculation, significant differences between treatments were determined by comparing abundances over time using ANOVAR, followed by a Dunnett's multiple comparisons test [74]. All data was tested to ensure that it passed the assumptions for normality and sphericity prior to running the ANOVAR.

Physiological Assays

Propidium iodide (PI) was used to quantitatively discriminate cell cycle stage in HHQ-exposed phytoplankton cultures over 122 h. Three replicate 2 L cultures at ~33,000 cells ml^{-1} were dosed with either 100 ng ml^{-1} HHQ or vehicle control (0.002% DMSO). Fixed cells were enumerated every 24 h via flow cytometry. Every 2 h, approximately 10^6 cells were subsampled, pelleted, and washed twice via centrifugation at 3,214 x *g* for 15 minutes at 18 °C. The dry cell

pellets were resuspended in 1 ml of ice-cold LCMS-grade methanol, transferred to microcentrifuge tubes and stored at -80 °C. To read, methanol-fixed cells were centrifuged at 16,000 x *g* for 10 minutes at 4 °C, methanol removed, and pellets were resuspended in 1 ml of 1X DPBS before re-pelleting by centrifugation at 16,000 x *g* for 10 minutes at 4 °C. The pellet was resuspended in 0.5 ml of FxCycle PI/RNAse solution (Thermo Fisher) and incubated for 30 minutes in the dark and then measured via flow cytometry (583/26 nm emission).

Diagnostic fluorescent dye assays were used to measure indicators of cell stress and programed cell death (PCD) following HHQ treatment. Intercellular reactive oxygen species (ROS), nitric oxide (NO) production, mitotoxicity, cytotoxicity, and quantification of caspase proteases and activity in whole-cell lysate were measured in *E. huxleyi* (starting cell concentration ~100,000 cells ml^{-1}) following HHQ treatment (70 ng ml^{-1} or 100 ng ml^{-1}) at various time points up to 72 h post-exposure. See Supplemental Information Text for detailed protocols.

E. huxleyi DNA integrity was examined using a modified protocol for the Click-iT TUNEL Alexa Fluor 488 Imaging Assay kit (Thermo Fisher). Four replicate *E. huxleyi* cultures (~ 250,000 cells ml^{-1}) were assayed using the manufacturer protocol and were sampled after 46 h HHQ exposure, with tagged cells enumerated via flow cytometry (512/18 nm emission). See Supplemental Information Text for detailed protocols.

Transmission Electron Microscopy

Replicate 20 ml cultures of exponentially growing *E. huxleyi* (~100,000 cells ml^{-1}) were exposed to either 100 ng ml^{-1} HHQ or vehicle control (0.2% DMSO) for 24 h. Samples were concentrated by filtration on a 0.45 µm polycarbonate filter and transitioned out of f/2 media via

three sequential washes with 10 ml of 0.2 M sodium cacodylate buffer pH 7.2, then fixed in 2% glutaraldehyde in 0.2 M sodium cacodylate buffer, pH 7.2. Samples were post-fixed in 2.0% osmium tetroxide for 1 h at room temperature and rinsed in DH_2O prior to *en bloc* staining with 2% uranyl acetate. After dehydration through a graded ethanol series, the cells were infiltrated and embedded in Embed-812 (Electron Microscopy Sciences). Thin sections were stained with uranyl acetate and lead citrate and examined with a JEOL 1010 electron microscope fitted with at Hamamatsu digital camera and AMT Advantage NanoSprint500 software.

Transcriptomic and Proteomic Analysis

A large-scale culturing experiment was performed with axenic *E. huxleyi* treated with either three concentrations of HHQ (1 ng ml^{-1}, 10 ng ml^{-1}, 100 ng ml^{-1}) or vehicle control (0.002% DMSO) for 72 h. Following HHQ/DMSO exposure, 400 ml subsamples were taken from each quadruplicate 2 L bottle at both 24 and 72 h for total RNA isolation and an additional 1200 ml subsample was taken at 72 h for total protein isolation. Total RNA and protein were isolated and quantified as described in Supplemental Information Text.

For RNA-seq analysis, the KAPA Stranded mRNA-Seq library preparation kit (Kapa Biosystems) was used to prepare library samples and sequenced on the NextSeq platform (Illumina) to generate 75 bp paired-end reads. Low-quality reads and adaptor sequences were trimmed using Trimmomatic (V0.38; [75]). Transcript abundances were determined using *Salmon* (V0.12.0; [76]) and the Ensembl [77] gene predictions for *E. huxleyi* CCMP1516 (the non-axenic form of CCMP2090; ftp://ftp.ensemblgenomes.org/pub/protists/release-41/fasta/emiliania_huxleyi/cdna/) as a transcript target index (k-mer size = 23). Normalization and determination of significantly differentially abundant transcripts was preformed using the

DESeq2 R package (V1.22.1; [78]). Tests for differential expression were carried out with the Wald test using a negative binomial generalized linear model. Logarithmic fold change (LFC) estimates were shrunken using the apeglm package (V1.6.0; [79]) within DESeq2. Resulting *p* values were adjusted using the Benjamini-Hochberg (BH) procedure (see Supplemental Information Text).

For proteomic analysis, proteins were solubilized in urea, reduced, alkylated, and trypsin digested following [80]. Resulting peptides samples were desalted with a mini-centrifugal C18 column following manufacturer's instructions (Nest Group). Peptides were chromatographically separated (precolumn: 3 cm, 100 μm i.d.; analytical column: 30 cm x 75 μm i.d; resin: 3 μm C18-AQ) with a nanoAcquity UPLC System (2–35% ACN, 0.1% v/v formic acid; 250 nl min-1, 90 minute) directly in line with a Fusion Lumos Orbitrap Tribrid mass spectrometer (Thermo Fisher Scientific) operated in data independent acquisition mode (DIA) following methods in [81]. To generate a peptide spectral library, 1 μg of a pooled sample containing equal parts from each peptide digest was analyzed with six gas phase fractions covering 400-1000 m/z in 100 m/z increments (4 m/z staggered MS2 windows, 2m/z overlap). Each bioreplicate was then quantified in single DIA analyses (MS1: 400-1000 m/z; 8 m/z staggered MS2 windows, 4m/z overlap).

In order to generate absolute abundance measurements of detected proteins, raw MS data files were processed using msconvert (ProteoWizard) for demultiplexing and peak picking. EncyclopeDIA (V0.7.4) was used to 1) search resulting fragmentation spectra against the UniProt *E. huxleyi* CCMP1516 protein and contaminant database (10.0 ppm precursor, fragment, and library tolerances), 2) provide peptide-level area under the curve (AUC) data, and 3) generate quantitative reports of identified peptides and proteins for each HHQ MS experiment

(1% false discovery rate). Significant changes ($q < 0.05$) in protein abundances between HHQ treatment and vehicle control were calculated as log2 fold-change between treatments. Complete details of protein sample preparations, chromatographic separations, mass spectrometry detection and quantification can be found in Supplemental Information Text.

Proteomic data were matched to the transcriptomic data utilizing corresponding NCBI accession numbers. As many of the genes and proteins were uncharacterized. Potential homologs of known proteins of interest were identified by querying the amino acid sequences of selected human proteins against the translated *E. huxleyi* (CCMP2090) genome, utilizing a significance threshold of E-value < 1 x 10^{-20}. Combined data were visualized utilizing the *ggplot2* and *pheatmap* packages in R.

PARP Inhibition and Homology Modelling

To examine the impact of alkylquinolone exposure on mammalian PARP activity, an inhibition assay was performed using the PARP Universal Colorimetric Assay Kit (R&D systems) according to the manufacturer instructions. Human PARP enzyme (0.5 U) was exposed to 50 μM HHQ (N = 4), 50 μM PQS (N = 4), or vehicle control (0.25% DMSO) (N = 4) for 15 min prior to the addition of a PARP activity buffer. See Supplemental Information Text for a detailed protocol.

The *E. huxleyi* sequence XP_005783504.1 was aligned to the Protein Data Bank (PDB) database to determine the closest structural homolog with a small molecular inhibitor veliparib in the active site that could lend insight into HHQ binding.

Detection of HHQ in Environmental Samples

Seawater samples were collected along a cruise track from Manta, Ecuador to Tahiti from October to December 2013 (US GEOTRACES EPZT GP16) as described previously [82]. Briefly, seawater was collected at 3 m depth by a tow-fish and pumped at a flow rate of 250 ml min^{-1} through a 0.2 μm filter and a polytetrafluoroethylene column packed with 20 g of polystyrene resin (Bondesil ENV; Agilent). Each sample represents an integrated average of 400-600 L of water across a wide region. Samples were frozen onboard at −20 °C. Prior to analysis, thawed columns were rinsed with 500 ml of 18.2 MΩ cm ultra-high purity water (qH_2O) and eluted with 250 ml of LCMS grade methanol. The extracts were concentrated by rotary evaporation and brought up in a final volume of 6 ml of qH_2O that was stored at -20°C. The organic extracts were separated by high pressure liquid chromatography (Dionex Ultimate 3000) coupled to an Orbitrap Fusion MS (Thermo Scientific), with specific methodology found in the Supplemental Information Text.

Acknowledgements

We acknowledge the support from the Electron Microscopy Resource Laboratory at the University of Pennsylvania for TEM sample processing. We thank Kay Bidle for thoughtful feedback on a previous draft of the manuscript and the viral cultures, Vinayak Agarwal for homology modeling support and discussions, Bradley Moore for tetrabromopyrrole, and Katie Barott for flow cytometry support. We thank members of the Whalen Laboratory including Ellysia Overton, Yongjie Gao, Carlotta Pazzi, Megan Coolahan, Shreya Kishore, Lucy Zhao for assistance in phytoplankton sampling for RNA and protein isolation and constructive discussions. We thank the Georgia Genomics and Bioinformatics Core facility for RNA

552 sequencing. Funding for this work was supported by the NSF grant (OCE-1657808) awarded to
553 K.E.W. and E.L.H. K.E.W. was also supported by a Faculty Research Grant from Haverford
554 College as well as funding from the Koshland Integrated Natural Science Center and Green Fund
555 at Haverford College. E.L.H. was also supported by a Sloan Foundation Research Fellowship.
556 B.L.N was supported by NSF grant (OCE-1633939). M.C.M. was supported by a NIH training
557 grant (T32 HG000035). Mass spectrometry was partially supported by the University of
558 Washington Proteomics Resource (UWPR95794). D.R. was supported by funding through the
559 Gordon and Betty Moore Foundation (Grant 6000), the Simons Collaboration for Ocean
560 Processes and Ecology Grant (329108), and an NSF grant (OCE-1736280). R.B. was supported
561 by an NSF Graduate Research Fellowship and an NSF grant (OCE-1829761).
562

563 **Data Deposition Statement**

564 Sequences from this study have been deposited in the Gene Expression Omnibus and are
565 accessible through GEO Series accession number GSE131846
566 (https://www.ncbi.nlm.nih.gov/geo/query/acc.cgi?acc=GSE131846). The raw mass spectrometry
567 proteomics data and subsequent spectral libraries have been deposited to the ProteomeXchange
568 Consortium via the PRIDE partner repository
569 (https://www.ebi.ac.uk/pride/archive/projects/PXD011560).

570 **REFERENCES**

571 1. Azam, F. and F. Malfatti, *Microbial structuring of marine ecosystems.* Nat Rev
572 Microbiol, 2007. **5**(10): p. 782-91.
573 2. Buchan, A., et al., *Master recyclers: features and functions of bacteria associated with*
574 *phytoplankton blooms.* Nature Reviews Microbiology, 2014. **12**(10): p. 686-698.
575 3. Cole, J.J., *Interactions between Bacteria and Algae in Aquatic Ecosystems.* Annual
576 Review of Ecology and Systematics, 1982. **13**: p. 291-314.
577 4. Fukami, K., et al., *Continuous culture with deep seawater of a benthic food diatom*
578 *Nitzschia sp.* Hydrobiologia, 1997. **358**: p. 245-249.
579 5. Danger, M., et al., *Bacteria can control stoichiometry and nutrient limitation of*
580 *phytoplankton.* Functional Ecology, 2007. **21**(2): p. 202-210.
581 6. Azam, F., et al., *The Ecological Role of Water-Column Microbes in the Sea.* Marine
582 Ecology Progress Series, 1983. **10**(3): p. 257-263.
583 7. Mayali, X. and F. Azam, *Algicidal bacteria in the sea and their impact on algal blooms.*
584 Journal of Eukaryotic Microbiology, 2004. **51**(2): p. 139-144.
585 8. Nealson, K.H., T. Platt, and J.W. Hastings, *Cellular control of the synthesis and activity*
586 *of the bacterial luminescent system.* J Bacteriol, 1970. **104**(1): p. 313-22.
587 9. Hmelo, L.R., *Quorum Sensing in Marine Microbial Environments.* Ann Rev Mar Sci,
588 2017. **9**: p. 257-281.
589 10. Reen, F.J., G.P. McGlacken, and F. O'Gara, *The expanding horizon of alkyl quinolone*
590 *signalling and communication in polycellular interactomes.* FEMS Microbiol Lett, 2018.
591 **365**(9).

11. Deziel, E., et al., *Analysis of Pseudomonas aeruginosa 4-hydroxy-2-alkylquinolines (HAQs) reveals a role for 4-hydroxy-2-heptylquinoline in cell-to-cell communication.* Proc Natl Acad Sci U S A, 2004. **101**(5): p. 1339-44.
12. Reen, F.J., et al., *The Pseudomonas quinolone signal (PQS), and its precursor HHQ, modulate interspecies and interkingdom behaviour.* Fems Microbiology Ecology, 2011. **77**(2): p. 413-428.
13. Mashburn, L.M. and M. Whiteley, *Membrane vesicles traffic signals and facilitate group activities in a prokaryote.* Nature, 2005. **437**(7057): p. 422-5.
14. Freund, J.R., et al., *Activation of airway epithelial bitter taste receptors by Pseudomonas aeruginosa quinolones modulates calcium, cyclic-AMP, and nitric oxide signaling.* J Biol Chem, 2018. **293**(25): p. 9824-9840.
15. Whalen, K.E., et al., *Bacterial alkylquinolone signaling contributes to structuring microbial communities in the ocean.* Microbiome, 2019. **7**.
16. Harvey, E.L., et al., *A Bacterial Quorum-Sensing Precursor Induces Mortality in the Marine Coccolithophore, Emiliania huxleyi.* Frontiers in Microbiology, 2016. **7**(59).
17. Pokrzywinski, K.L., et al., *Cell cycle arrest and biochemical changes accompanying cell death in harmful dinoflagellates following exposure to bacterial algicide IRI-160AA.* Sci Rep, 2017. **7**: p. 45102.
18. van Tol, H.M., S.A. Amin, and E.V. Armbrust, *Ubiquitous marine bacterium inhibits diatom cell division.* ISME J, 2017. **11**(1): p. 31-42.
19. McKew, B.A., et al., *Acclimation of Emiliania huxleyi (1516) to nutrient limitation involves precise modification of the proteome to scavenge alternative sources of N and P.* Environ Microbiol, 2015. **17**(10): p. 4050-62.

20. Parpais, J., et al., *Effect of phosphorus starvation on the cell cycle of the photosynthetic prokaryote Prochlorococcus spp.* Marine Ecology Progress Series, 1996. **132**(1-3): p. 265-274.
21. Rokitta, S., et al., *P- and N-depletion trigger similar cellular responses to promote senescence in eukaryotic phytoplankton.* Frontiers in Marine Science, 2016. **3**: p. 109.
22. Vaulot, D., et al., *Cell-Cycle Response to Nutrient Starvation in 2 Phytoplankton Species, Thalassiosira-Weissflogii and Hymenomonas-Carterae.* Marine Biology, 1987. **95**(4): p. 625-630.
23. Mojica, K.D. and C.P. Brussaard, *Factors affecting virus dynamics and microbial host-virus interactions in marine environments.* FEMS Microbiol Ecol, 2014. **89**(3): p. 495-515.
24. Balch, W.M., P.M. Holligan, and K.A. Kilpatrick, *Calcification, Photosynthesis and Growth of the Bloom-Forming Coccolithophore, Emiliania-Huxleyi.* Continental Shelf Research, 1992. **12**(12): p. 1353-1374.
25. Simo, R., *Production of atmospheric sulfur by oceanic plankton: biogeochemical, ecological and evolutionary links.* Trends Ecol Evol, 2001. **16**(6): p. 287-294.
26. Guillard, R.R.L., *Culture of phytoplankton for feeding marine invertebrates*, in *Culture of marine invertebrate animals.* W.L. Smith and M.H. Chaney, Editors. 1975, Plenum Press. p. 29-60.
27. Barak-Gavish, N., et al., *Bacterial virulence against an oceanic bloom-forming phytoplankter is mediated by algal DMSP.* Sci Adv, 2018. **4**(10): p. eaau5716.
28. Bramucci, A.R. and R.J. Case, *Phaeobacter inhibens induces apoptosis-like programmed cell death in calcifying Emiliania huxleyi.* Sci Rep, 2019. **9**(1): p. 5215.

29. Segev, E., et al., *Dynamic metabolic exchange governs a marine algal-bacterial interaction.* Elife, 2016. **5**.
30. Shemi, A., et al., *Phosphorus starvation induces membrane remodeling and recycling in Emiliania huxleyi.* New Phytol, 2016. **211**(3): p. 886-98.
31. Dyhrman, S.T., *Nutrients and their acquisition: Phosphorus physiology in microalgae*, in *The Physiology of Microalgae. Developments in Applied Phycology*, M. Borowitzka, J. Beardall, and J. Raven, Editors. 2016, Springer, Cham. p. 155-183.
32. Dyhrman, S.T. and K.C. Ruttenberg, *Presence and regulation of alkaline phosphatase activity in eukaryotic phytoplankton from the coastal ocean: Implications for dissolved organic phosphorus remineralization.* Limnology and Oceanography, 2006. **51**(3): p. 1381-1390.
33. Xu, Y., et al., *A novel alkaline phosphatase in the coccolithophore Emiliania huxleyi (Prymnesiophyceae) and its regulation by phosphorus.* Journal of Phycology, 2006. **42**(4): p. 835-844.
34. Bidle, K.D., *The molecular ecophysiology of programmed cell death in marine phytoplankton.* Ann Rev Mar Sci, 2015. **7**: p. 341-75.
35. Holban, A.M., et al., *Role of Pseudomonas aeruginosa quorum sensing (QS) molecules on the viability and cytokine profile of human mesenchymal stem cells.* Virulence, 2014. **5**(2): p. 303-10.
36. Chao, H.X., et al., *Orchestration of DNA Damage Checkpoint Dynamics across the Human Cell Cycle.* Cell Syst, 2017. **5**(5): p. 445-459 e5.
37. Limas, J.C. and J.G. Cook, *Preparation for DNA replication: the key to a successful S phase.* FEBS Lett, 2019. **593**(20): p. 2853-2867.

38. Ciardo, D., A. Goldar, and K. Marheineke, *On the Interplay of the DNA Replication Program and the Intra-S Phase Checkpoint Pathway.* Genes (Basel), 2019. **10**(2).
39. Christopher, A., et al., *Modelling Robust Feedback Control Mechanisms That Ensure Reliable Coordination of Histone Gene Expression with DNA Replication.* PLoS One, 2016. **11**(10): p. e0165848.
40. Pai, C.C. and S.E. Kearsey, *A Critical Balance: dNTPs and the Maintenance of Genome Stability.* Genes (Basel), 2017. **8**(2).
41. Lane, A.N. and T.W. Fan, *Regulation of mammalian nucleotide metabolism and biosynthesis.* Nucleic Acids Res, 2015. **43**(4): p. 2466-85.
42. Wu, Y. and M.R. Seyedsayamdost, *Synergy and Target Promiscuity Drive Structural Divergence in Bacterial Alkylquinolone Biosynthesis.* Cell Chem Biol, 2017. **24**(12): p. 1437-1444 e3.
43. Arnould, S., et al., *Checkpoint kinase 1 inhibition sensitises transformed cells to dihydroorotate dehydrogenase inhibition.* Oncotarget, 2017. **8**(56): p. 95206-95222.
44. Fairus, A.K.M., et al., *Dihydroorotate dehydrogenase (DHODH) inhibitors affect ATP depletion, endogenous ROS and mediate S-phase arrest in breast cancer cells.* Biochimie, 2017. **135**: p. 154-163.
45. Li, C. and J.T.Y. Wong, *DNA Damage Response Pathways in Dinoflagellates.* Microorganisms, 2019. **7**(7).
46. Vlcek, D., et al., *Chlamydomonas reinhardtii: a convenient model system for the study of DNA repair in photoautotrophic eukaryotes.* Curr Genet, 2008. **53**(1): p. 1-22.
47. Liu, L.C., et al., *Inactivation/deficiency of DHODH induces cell cycle arrest and programed cell death in melanoma.* Oncotarget, 2017. **8**(68): p. 112354-112370.

48. Jagtap, P. and C. Szabo, *Poly(ADP-ribose) polymerase and the therapeutic effects of its inhibitors.* Nature Reviews Drug Discovery, 2005. **4**(5): p. 421-440.

49. Wei, H.T. and X.C. Yu, *Functions of PARylation in DNA Damage Repair Pathways.* Genomics Proteomics & Bioinformatics, 2016. **14**(3): p. 131-139.

50. Yu, S.W., et al., *Mediation of poly(ADP-ribose) polymerase-1-dependent cell death by apoptosis-inducing factor.* Science, 2002. **297**(5579): p. 259-263.

51. Noel, G., et al., *Radiosensitization by the poly(ADP=ribose) polymerase inhibitor 4-amino-1,8-naphthalimide is specific of the S phase of the cell cycle and involves arrest of DNA syntheses.* Molecular Cancer Therapeutics, 2006. **5**(3): p. 564-574.

52. Abdullah, I., et al., *Benzimidazole derivatives as potential dual inhibitors for PARP-1 and DHODH.* Bioorganic & Medicinal Chemistry, 2015. **23**(15): p. 4669-4680.

53. Milanese, C., et al., *DNA damage and transcription stress cause ATP-mediated redesign of metabolism and potentiation of anti-oxidant buffering.* Nat Commun, 2019. **10**(1): p. 4887.

54. Chang, H.C. and L. Guarente, *SIRT1 and other sirtuins in metabolism.* Trends Endocrinol Metab, 2014. **25**(3): p. 138-45.

55. Canto, C., K.J. Menzies, and J. Auwerx, *NAD(+) Metabolism and the Control of Energy Homeostasis: A Balancing Act between Mitochondria and the Nucleus.* Cell Metab, 2015. **22**(1): p. 31-53.

56. Bai, P., et al., *PARP-1 inhibition increases mitochondrial metabolism through SIRT1 activation.* Cell Metab, 2011. **13**(4): p. 461-468.

57. Webster, B.R., et al., *The role of sirtuins in modulating redox stressors.* Free Radic Biol Med, 2012. **52**(2): p. 281-90.

58. Legendre, C., et al., *Pseudomonas aeruginosa Alkyl quinolones repress hypoxia-inducible factor 1 (HIF-1) signaling through HIF-1alpha degradation.* Infect Immun, 2012. **80**(11): p. 3985-92.
59. Flamholz, A., et al., *Glycolytic strategy as a tradeoff between energy yield and protein cost.* Proc Natl Acad Sci U S A, 2013. **110**(24): p. 10039-44.
60. Patel, D., et al., *Aspartate Rescues S-phase Arrest Caused by Suppression of Glutamine Utilization in KRas-driven Cancer Cells.* J Biol Chem, 2016. **291**(17): p. 9322-9.
61. Kim, J., et al., *Effect of cell cycle arrest on intermediate metabolism in the marine diatom Phaeodactylum tricornutum.* Proc Natl Acad Sci U S A, 2017. **114**(38): p. E8007-E8016.
62. Bilgin, D.D., et al., *Biotic stress globally downregulates photosynthesis genes.* Plant Cell Environ, 2010. **33**(10): p. 1597-613.
63. Lodeyro, A.F., et al., *The importance of flavodoxin for environmental stress tolerance in photosynthetic microorganisms and transgenic plants. Mechanism, evolution and biotechnological potential.* FEBS Lett, 2012. **586**(18): p. 2917-24.
64. Havaux, M., et al., *Vitamin B6 deficient plants display increased sensitivity to high light and photo-oxidative stress.* BMC Plant Biol, 2009. **9**: p. 130.
65. Ku, C., et al., *A single-cell view on alga-virus interactions reveals sequential transcriptional programs and infection states.* Sci Adv, 2020. **6**(21): p. eaba4137.
66. Sheyn, U., et al., *Modulation of host ROS metabolism is essential for viral infection of a bloom-forming coccolithophore in the ocean.* ISME J, 2016. **10**(7): p. 1742-54.
67. Bidle, K.D., et al., *Viral activation and recruitment of metacaspases in the unicellular coccolithophore, Emiliania huxleyi.* Proceedings of the National Academy of Sciences of the United States of America, 2007. **104**(14): p. 6049-6054.

730 68. Cooper, M.B. and A.G. Smith, *Exploring mutualistic interactions between microalgae*
731 *and bacteria in the omics age.* Curr Opin Plant Biol, 2015. **26**: p. 147-53.
732 69. Krupke, A., et al., *Quorum sensing plays a complex role in regulating the enzyme*
733 *hydrolysis activity of microbes associated with sinking particles in the ocean.* Frontiers in
734 Marine Science, 2016. **3**(55).
735 70. Sanudo-Wilhelmy, S.A., et al., *The role of B vitamins in marine biogeochemistry.* Ann
736 Rev Mar Sci, 2014. **6**: p. 339-67.
737 71. Kochany, J. and R.J. Maguire, *Photodegradation of Quinoline in Water.* Chemosphere,
738 1994. **28**(6): p. 1097-1110.
739 72. Seymour, J.R., et al., *Zooming in on the phycosphere: the ecological interface for*
740 *phytoplankton-bacteria relationships.* Nat Microbiol, 2017. **2**: p. 17065.
741 73. Becker, J.W., M.L. Brandon, and M.S. Rappe, *Cultivating microorganisms from dilute*
742 *aquatic environments: melding traditional methodology with new cultivation techniques*
743 *and molecular methods*, in *Manual of Environmental Microbiology*, C.J.H.e. al., Editor.
744 2007, ASM Press. p. 399-406.
745 74. Dunnett, C.W., *A Multiple Comparison Procedure for Comparing Several Treatments*
746 *with a Control.* Journal of the American Statistical Association, 1955. **50**(272): p. 1096-
747 1121.
748 75. Bolger, A.M., M. Lohse, and B. Usadel, *Trimmomatic: a flexible trimmer for Illumina*
749 *sequence data.* Bioinformatics, 2014. **30**(15): p. 2114-20.
750 76. Patro, R., et al., *Salmon provides fast and bias-aware quantification of transcript*
751 *expression.* Nat Methods, 2017. **14**(4): p. 417-419.

77. Kersey, P.J., et al., *Ensembl Genomes 2018: an integrated omics infrastructure for non-vertebrate species.* Nucleic Acids Res, 2018. **46**(D1): p. D802-D808.
78. Love, M.I., W. Huber, and S. Anders, *Moderated estimation of fold change and dispersion for RNA-seq data with DESeq2.* Genome Biology, 2014. **15**(12).
79. Zhu, A., J.G. Ibrahim, and M.I. Love, *Heavy-tailed prior distributions for sequence count data: removing the noise and preserving large differences.* Bioinformatics, 2018. **11**: p. R106.
80. Nunn, B.L., et al., *Proteomics of Colwellia psychrerythraea at subzero temperatures - a life with limited movement, flexible membranes and vital DNA repair.* Environ Microbiol, 2015. **17**(7): p. 2319-35.
81. Searle, B.C., et al., *Chromatogram libraries improve peptide detection and quantification by data independent acquisition mass spectrometry.* Nat Commun, 2018. **9**(1): p. 5128.
82. Boiteau, R.M., et al., *Siderophore-based microbial adaptations to iron scarcity across the eastern Pacific Ocean.* Proc Natl Acad Sci U S A, 2016. **113**(50): p. 14237-14242.

TABLES

Table 1. Summary of differentially expressed transcripts and proteins following HHQ exposure. Expression of each HHQ treatment was compared to expression in the vehicle control (DMSO) treatment (Welch's approximate t-test; *q*-value < 0.05).

	24 h			72 h		
	Up	Down	Unchanged	Up	Down	Unchanged
Transcript						
1 ng/mL	13	20	31,476	0	0	31,549
10 ng/mL	2,702	1,990	26,817	382	159	31,008
100 ng/mL	5,948	6,605	18,956	6,166	5,698	19,685
Protein						
1 ng/mL	n/a	n/a	n/a	0	0	5,528
10 ng/mL	n/a	n/a	n/a	3	0	5,525
100 ng/mL	n/a	n/a	n/a	628	375	4,525

FIGURES

Figure 1. Exposure to HHQ halts cell division and alters cell morphology. *E. huxleyi* cultures (N = 3) were exposed to HHQ or vehicle control (DMSO) at T_0 and monitored by flow cytometry for cell abundance (a), red fluorescence in RFUs (695/50 nm; a proxy for chlorophyll a intensity) (b), forward scatter (a proxy for cell size) (c), and side scatter (a proxy for cell granularity) (d) over 96 h. Mean ± standard deviation shown. In 100 ng ml^{-1} HHQ-exposed cells all parameters measured were significantly different from the vehicle control (repeated measures ANOVA; $p < 0.05$). Note, in part (a), data for HHQ-treated cells at 1 ng ml^{-1} sit directly beneath data for vehicle control (DMSO). Transmission electron microscopy micrographs of *E. huxleyi* cells exposed to vehicle control (DMSO; e) or 100 ng ml^{-1} HHQ (f) for 24 h. Subcellular structures

include chloroplast (c), lipid droplet (l), mitochondria (m), nucleus (n), vacuole (black arrow head).

Figure 2. HHQ triggers stalling in S-phase. Cell cycle stage was quantified by profiling fluorescence (575/25 nm), a proxy for DNA content, of propidium iodide stained *E. huxleyi* cultures (N = 3) exposed to either vehicle control (DMSO) (a) or 100 ng ml^{-1} HHQ (b) for 96 h. (c thru e) The proportion of cells in each cell stage was determined from density plots of the distribution of cells with varying DNA content ranging from 2N (G1, yellow) to 4N (G2, blue) at T0, T24, T48, T72, and T96 h. Cells with intermediate DNA content were denoted as S-phase (orange), as the genome replicated. Each plot represents the mean ± standard deviation for triplicate samples (ANOVAR, $p < 0.05$). (f) Comparison of mean fluorescence (575/25 mm) of G1 and S cells treated with vehicle control (DMSO) or 100 ng ml^{-1} HHQ for 96 h stained with propidium iodide were compared via Welch's approximate t-test, $p < 0.01$. As DNA replication only occurs in S-phase, the increase in mean fluorescence for HHQ-treated cells that fall within the G1 gate suggests that these cells are currently in S-phase, but stall early in the process of DNA synthesis and are unable to synthesize enough additional DNA to fall within the S-phase region.

Figure 3. Molecular and proteomic changes as a result of HHQ exposure. (a) Comparison of $\log_2$ fold changes in transcript (x-axis) and protein (y-axis) expression from *E. huxleyi* cultures (N = 4) following exposure to 100 ng ml-1 HHQ for 72 h compared to the vehicle control (DMSO). Only shared differentially expressed transcripts (Wald test, q-value < 0.05) and proteins (Welch's approximate t-test, q-value < 0.05) are shown for a total of 665 genes/proteins.

Transcripts and proteins with similar functions are colored via gene ontology (GO) annotation according to the curated groupings shown in **Supplemental Data File 1** at https://doi.org/10.6084/m9.figshare.14414285.v1. Genes and proteins without GO annotations or annotations outside of the selected groupings are shown in grey. Selected outliers are labeled in black. Heat maps displaying putative homologs of *E. huxleyi* protein coding genes associated with cell cycle regulation (b) and DNA damage repair response (c) after 72 h of HHQ exposure. Black boxes indicate proteins that were not detected in the proteomic analysis. Bolded names indicate those protein coding genes found within the scatterplot in part a. Dendrograms indicate hierarchical clustering based on similarity of gene/protein expression level.

Figure 4. Exposure to HHQ leads to cellular DNA damage and inhibition of human PARP. (a) Cultures (N = 4) of *E. huxleyi* were exposed to 100 ng ml^{-1} HHQ or the vehicle control (DMSO) for 46 h before pigments were removed and cells were stained using an *in vivo* TUNEL assay to detect presence of DNA ends, a proxy for DNA breaks. (b) Inhibition of human PARP-1 enzyme by 50 μM HHQ and 2-heptyl-3-hydroxy-4(1H)-quinolone (PQS). Percent PARP inhibition was measured using the PARP Universal Colorimetric Assay Kit (R&D systems). Theabsorbance values of quadruplicate wells containing HHQ or PQS were compared to the vehicle control and this ratio was subtracted from 100 percent to determine PARP inhibition. Points represent individual replicates. Asterisks indicate a significant difference between the treatment and the vehicle control (Welch's approximate t-test, p-value < 0.05).

Figure 5. HHQ can inhibit *E. huxleyi* viral-induced mortality. The abundance (cells ml^{-1}) of *E. huxleyi* over time (hours) after exposed to either the vehicle control (DMSO; black), HHQ (100

835 ng ml^{-1}; gray), EhV 207 (blue), or HHQ + EhV 207 (red; MOI = 80). (a) HHQ and the virus were
836 added together. (b) HHQ was added at T0, and the virus after 72 h. (c) Virus was added at T0,
837 and HHQ addition was delayed for 24 h. For each treatment in each experiment N = 3, and mean
838 ± standard deviation is shown.
839
840 **Figure 6.** A proposed model for the role of HHQ in influencing viral success in *E. huxleyi*.
841 During the infection of a phytoplankton cell (a), viruses are recognized via specific surface
842 receptors and will enter the cell via endocytosis through distinct lipid rafts. Once inside the cell,
843 the virus hijacks host replication machinery to produce additional viral particles. This replication
844 is dependent on functional *de novo* nucleotide synthesis enzymes, such as dihydroorotate
845 dehydrogenase (DHODH), to provide the cell with sufficient nucleotide materials. Likewise,
846 functional DNA repair, often mediated by poly(ADP-ribose) polymerase (PARP), is necessary to
847 ensure replication can continue. Successful viral replication then generates intracellular reactive
848 oxygen species (ROS) and nitric oxide (NO) signaling, which in turn activates caspase proteases
849 allowing for the release of replicated viral particles via programmed cell death (PCD) induced
850 cell lysis. In HHQ-exposed phytoplankton cells (b), virus-induced mortality was not observed,
851 but the mechanism by which HHQ is impacting viral cycling remains unclear. HHQ may directly
852 inhibit (shown as red lines) the activity of DHODH and PARP, which would prevent the
853 production of viral particles via the collapse of DNA replication machinery. HHQ may also
854 indirectly impact parts of the virus cycle (shown as dotted lines), by changing host physiology to
855 disrupt recognition, nucleotide production, ROS production, caspase activation, or PCD.
856
857 **Supplemental Material**

Supplemental Information Text. File contains additional methodological information.

Supplemental Figure 1. Composite TEM images showing representative images of *E. huxleyi* cells exposed to (a through f) vehicle control (DMSO) or (g through l) 100 ng ml^{-1} HHQ for 24 h. In select images subcellular structures have been labeled for identification. Chloroplast (c), lipid droplet (l), mitochondria (m), nucleus (n), pyrenoid (p), golgi (black arrow), vacuole (v), and vesicles (white arrowheads). Scale bar = 500 nm.

Supplemental Figure 2. *E. huxleyi* cultures were examined for their ability to recover following exposure to 100 ng ml^{-1} of HHQ for 96 h. Following HHQ exposure, cultures were monitored for their ability to recover by measuring growth rate (a; each point represents the exponential growth rate over the previous 24 h), red fluorescence in RFUs (a proxy for chlorophyll a intensity) (b), and forward scatter (a proxy for cell size) (c). Each symbol represents the mean of three independent replicates ± standard deviation. Significant differences between HHQ-exposed cells and the vehicle control were assessed using an ANOVAR ($p < 0.05$).

Supplemental Figure 3. (a) Principal component analysis performed on the regularized-logarithm transformed transcriptomic read counts matrix. Each point represents an experimental sample with point color indicating treatment and shape indicating the time point. The first component explains 39% of variance and the second component explains 20%. (b) Principal component analysis performed on logarithm transformed proteomic data matrix (protein summed peptide peak area values +1). Each point represents an experimental sample with point color

indicating treatment. The first component explains 29.8% of variance and the second component explains 16.2%. Note, protein was only collected at the 72 hr. (c) Growth curve of *E. huxleyi* (2090, axenic) cultures exposed to 1, 10, and 100 ng mL^{-1} HHQ and sampled for RNA (at 24 and 72 h) and protein (at 72 h). The arrow indicates time of HHQ addition.

Supplemental Figure 4. Diagnostic biochemical assays for (a) caspase activity from whole-cell lysates or purified caspase enzyme (N = 3; comparison of whole cell lysate at 72 hr DMSO versus whole cell lysate at 72 hr HHQ; Welch's approximate t-test, p-value < 0.05; no significance observed), (b) the presence of active caspase proteases *in vivo* (CaspACE), (c) reactive nitrogen species (DAF-FM Diacetate), (d) reactive oxygen species (CM-H_2DCFDA) from DMSO or HHQ-exposed cultures from 1 to 72 h post-treatment, (e) reactive oxygen species (CM-H_2DCFDA) from 72 h DMSO or HHQ-exposed cultures that were spiked with the algicide tetrabromopyrrole (TBP, positive control) for 1 or 2 h, (f) apoptosis (Image-iT DEAD stain) from DMSO or HHQ-exposed cultures from 1 to 72 h post-treatment, (g) apoptosis (Image-iT DEAD stain) from 72 h DMSO or HHQ-exposed cultures that were spiked with TBP (positive control) for 4.5 h, and (f) mitochondrial membrane integrity (MitoHealth Stain). Bars represent the mean ± standard deviation of triplicate readings. Significance (part b, c, d, f, h) based on ANOVAR, Dunnett's multiple comparisons test, p-value < 0.05. Significance (part e, g) based on Student's t-test, p-value < 0.05. Cells exposed to HHQ were only significantly different from the control using the MitoHealth stain after 24 h of exposure. However, the two treatments were not significantly different from one another at all subsequent time points.

Supplemental Figure 5. HHQ does not directly lead to DNA strand breaks. Lambda DNA and genomic DNA isolated from *E. huxleyi* CCMP2090 was incubated with 100 ng ml^{-1} HHQ or the volumetric equivalent of DMSO for 24 h at 18°C, and the presence of DNA strand breaks was assessed by agarose gel stained with ethidium bromide.

Supplemental Figure 6. Impact of alkylquinolones on phytoplankton growth and protein homology modeling. (a) Effect of PQS on *E. huxleyi* growth. Dose-response curve of *E. huxleyi (*strain 2090, axenic) in response to PQS. Each symbol represents the mean of three independent replicates ± standard deviation. Protein homology modeling of *E. huxleyi* PARP1-like homolog (XP_005783504.1) to the crystal structure of human PARP1 (PDB 2RD6) with the PARP inhibitor veliparib. (b) The sequence of *E. huxleyi* PARP-like homolog (XP_005783504.1) was aligned to human PARP1 (PDB 2RD6). Two key amino acid residues (red), the Tyr and Glu, are strictly conserved between human PARP and *E. huxleyi* protein. (c, d) The active site of PDB 2RD6 shows the binding of the inhibitor veliparib. Regions in 2RD6 with greatest homology to *E. huxleyi* PARP-like homolog are colored in pink with the remainder of the protein chain in green. The region comprising the active site for small molecule binding is highly conserved between the two proteins with two key binding interactions observed – the near co-planar arrangement of a tyrosine side chain phenyl to the inhibitor, and a water mediated hydrogen bond of the basic nitrogen atom of the inhibitor to a glutamate side chain carboxyl.

Supplemental Figure 7. Detection of HHQ in the marine environment. (a) Cruise track of the U.S. GEOTRACES GP16 cruise in 2013 in the eastern southern tropical Pacific Ocean. (b) Grey bars indicated the concentration of HHQ from six stations along the cruise track. Circles indicate

925 the percent relative abundance picoplankton (yellow) and micro- & nanoplankton (red).
926 Previously, HHQ has been isolated from laboratory cultures of both marine *Pseudoalteromonas*
927 and *Pseudomonas* spp. Composite figure showing the detection of HHQ in environmental
928 samples. The extracted ion chromatograms for HHQ ($[M+H]^+$ = 244.17 *m/z*) detected by high-
929 resolution (450K) orbitrap LC-ESIMS for the standard (c) and environmental samples (d). HHQ
930 confirmation via MS/MS analysis in environmental samples compared to an authentic standard.
931 High mass accuracy HCD fragmentation spectra (35% collision energy) of the $[M+H]^+$ ion were
932 collected at 38 minutes (e).
933

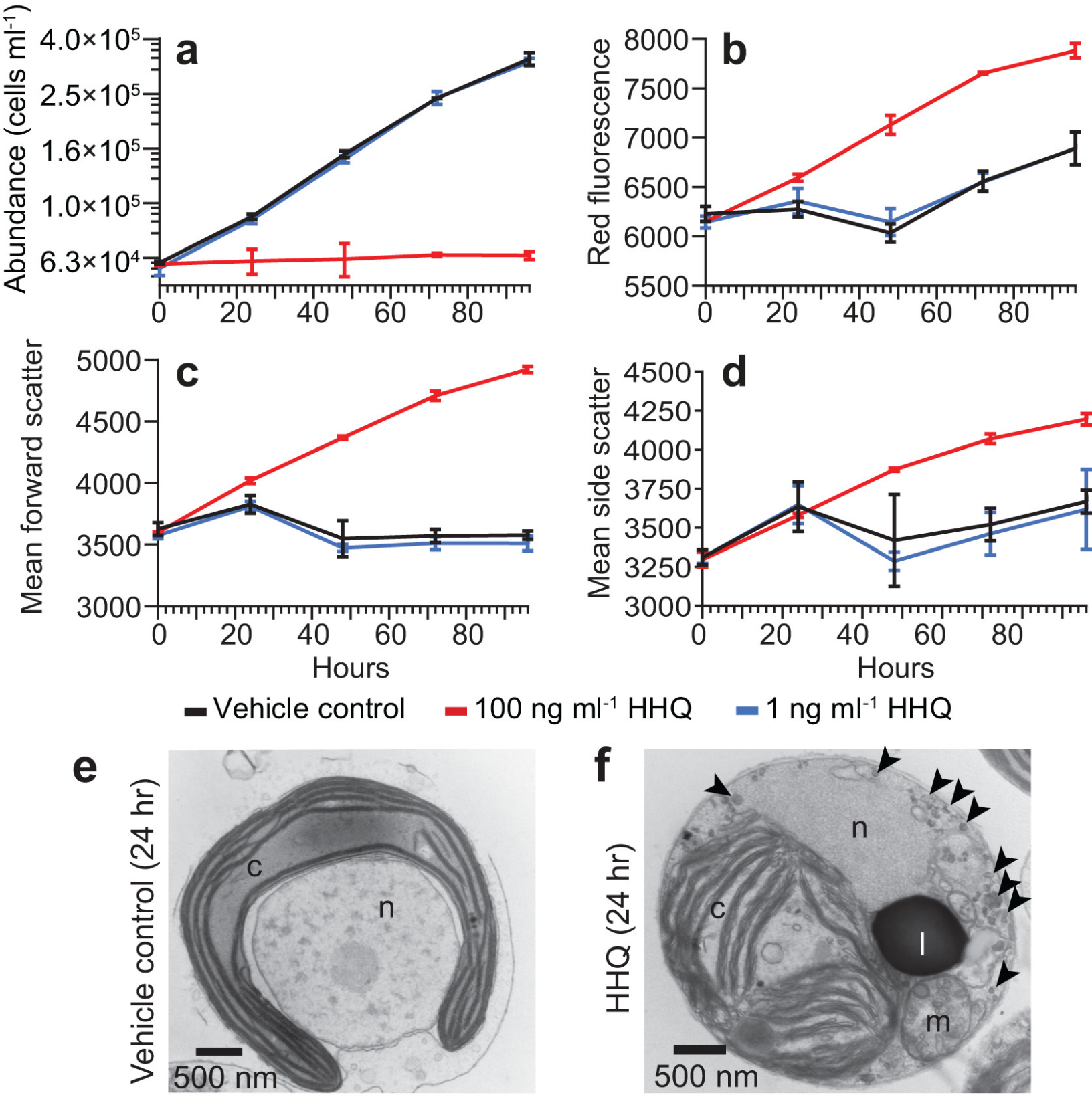
a
b
c
d
e
f
Abundance (cells ml-1)
4.0×10^5
2.5×10^5
1.6×10^5
1.0×10^5
6.3×10^4
Red fluorescence
8000
7500
7000
6500
6000
5500
Mean forward scatter
5000
4500
4000
3500
3000
Mean side scatter
4500
4250
4000
3750
3500
3250
3000
0
20
40
60
80
Hours
Vehicle control
100 ng ml-1 HHQ
1 ng ml-1 HHQ
Vehicle control (24 hr)
HHQ (24 hr)
c
n
l
m
500 nm

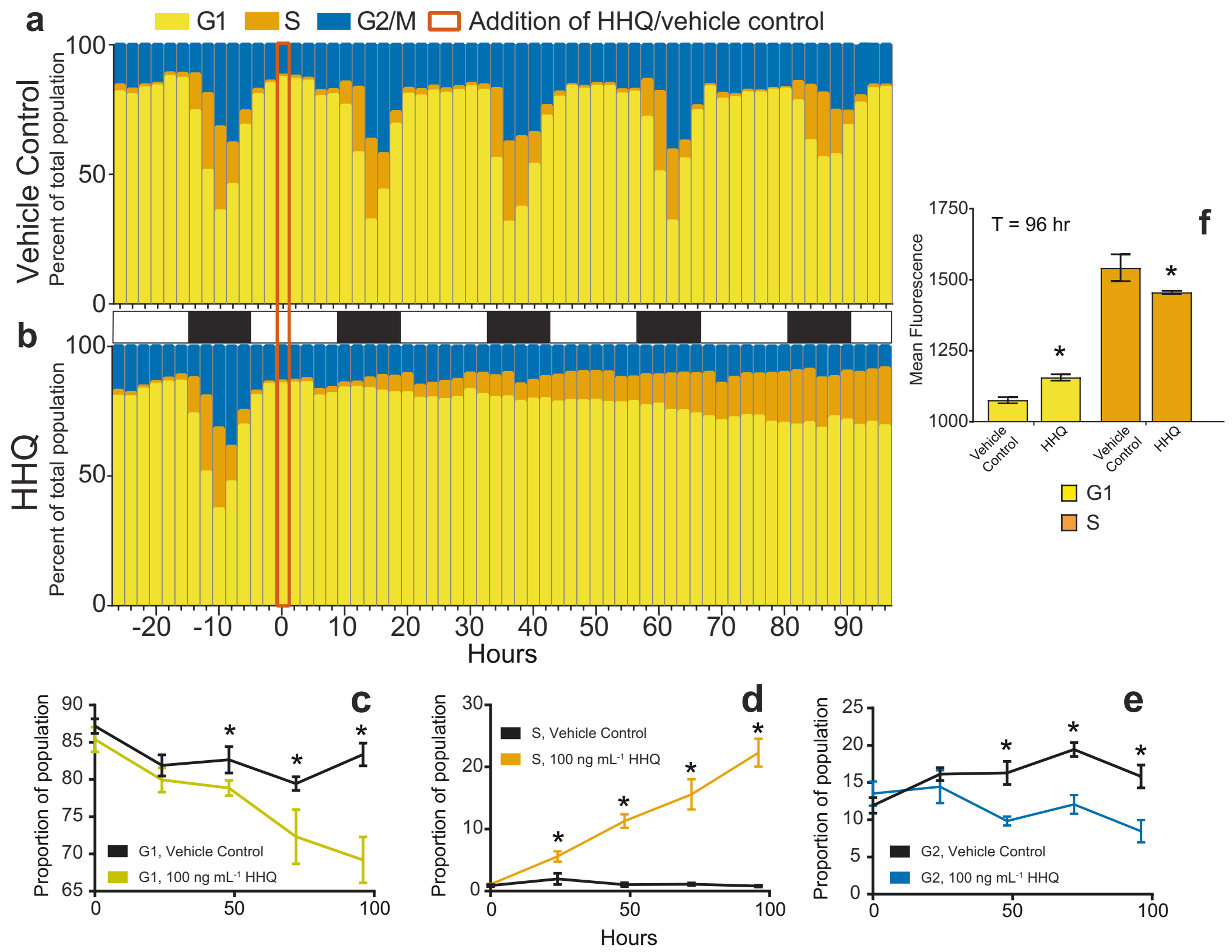
a
G1
S
G2/M
Addition of HHQ/vehicle control
Vehicle Control
Percent of total population
100
50
0
b
HHQ
Percent of total population
100
50
0
-20
-10
0
10
20
30
40
50
60
70
80
90
Hours
f
T = 96 hr
Mean Fluorescence
1750
1500
1250
1000
Vehicle Control
HHQ
Vehicle Control
HHQ
G1
S
c
Proportion of population
90
85
80
75
70
65
G1, Vehicle Control
G1, 100 ng mL-1 HHQ
0
50
100
d
Proportion of population
30
20
10
0
S, Vehicle Control
S, 100 ng mL-1 HHQ
0
50
100
Hours
e
Proportion of population
25
20
15
10
5
0
G2, Vehicle Control
G2, 100 ng mL-1 HHQ
0
50
100

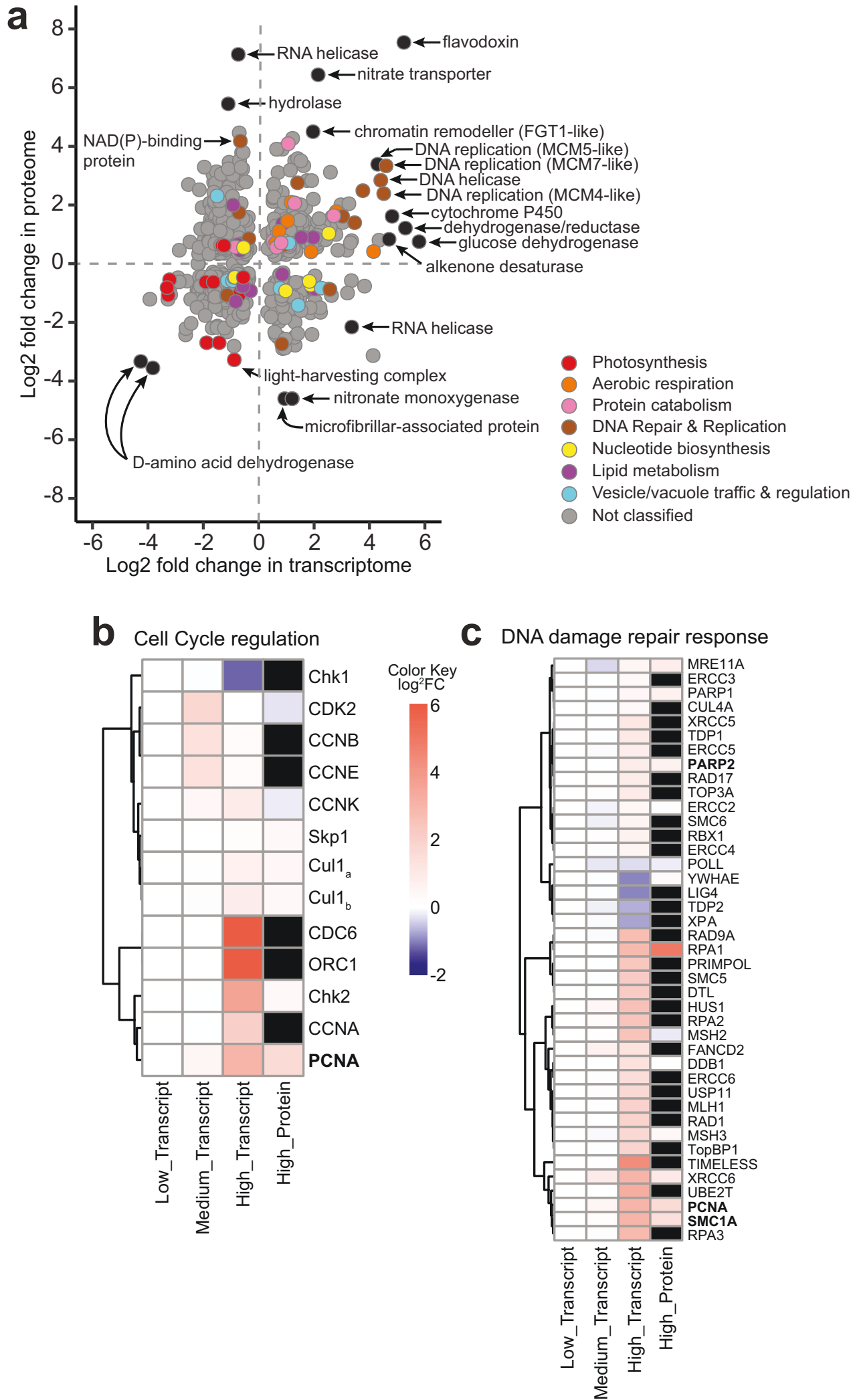
a
Log2 fold change in proteome
Log2 fold change in transcriptome
flavodoxin
RNA helicase
nitrate transporter
hydrolase
chromatin remodeller (FGT1-like)
NAD(P)-binding protein
DNA replication (MCM5-like)
DNA replication (MCM7-like)
DNA helicase
DNA replication (MCM4-like)
cytochrome P450
dehydrogenase/reductase
glucose dehydrogenase
alkenone desaturase
RNA helicase
light-harvesting complex
nitronate monoxygenase
microfibrillar-associated protein
D-amino acid dehydrogenase
Photosynthesis
Aerobic respiration
Protein catabolism
DNA Repair & Replication
Nucleotide biosynthesis
Lipid metabolism
Vesicle/vacuole traffic & regulation
Not classified
b
Cell Cycle regulation
Color Key log2FC
Chk1
CDK2
CCNB
CCNE
CCNK
Skp1
Cul1a
Cul1b
CDC6
ORC1
Chk2
CCNA
PCNA
Low_Transcript
Medium_Transcript
High_Transcript
High_Protein
c
DNA damage repair response
MRE11A
ERCC3
PARP1
CUL4A
XRCC5
TDP1
ERCC5
PARP2
RAD17
TOP3A
ERCC2
SMC6
RBX1
ERCC4
POLL
YWHAE
LIG4
TDP2
XPA
RAD9A
RPA1
PRIMPOL
SMC5
DTL
HUS1
RPA2
MSH2
FANCD2
DDB1
ERCC6
USP11
MLH1
RAD1
MSH3
TopBP1
TIMELESS
XRCC6
UBE2T
PCNA
SMC1A
RPA3
Low_Transcript
Medium_Transcript
High_Transcript
High_Protein

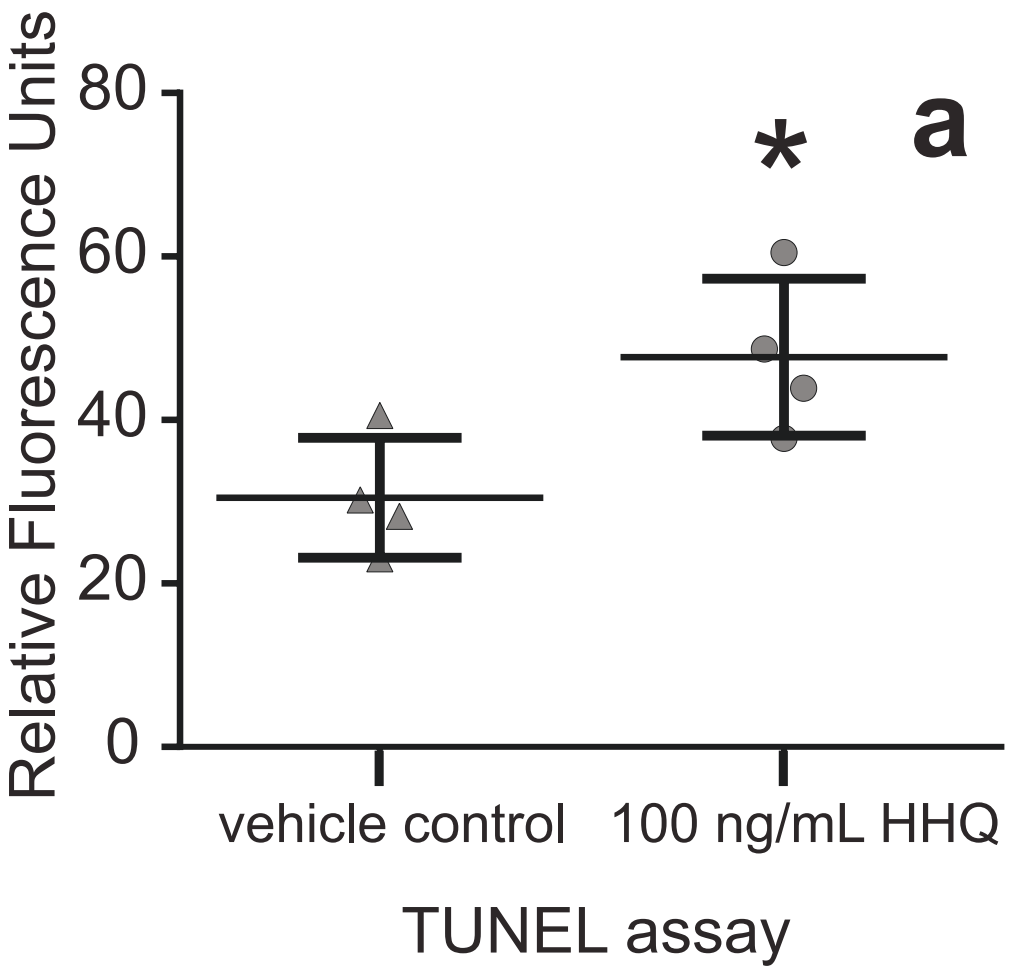
Relative Fluorescence Units
80
60
40
20
0
*
a
vehicle control
100 ng/mL HHQ
TUNEL assay

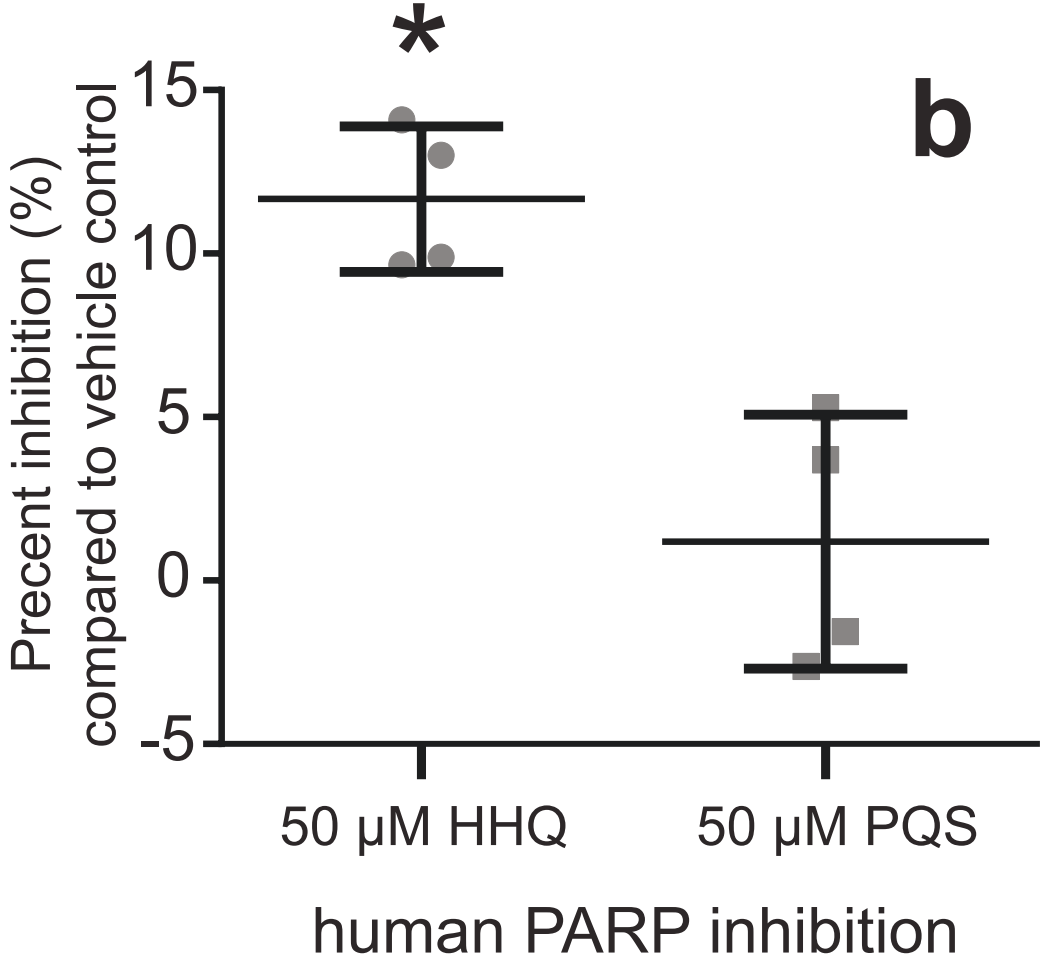
Precent inhibition (%)
compared to vehicle control
15
10
5
0
-5
*
b
50 µM HHQ
50 µM PQS
human PARP inhibition

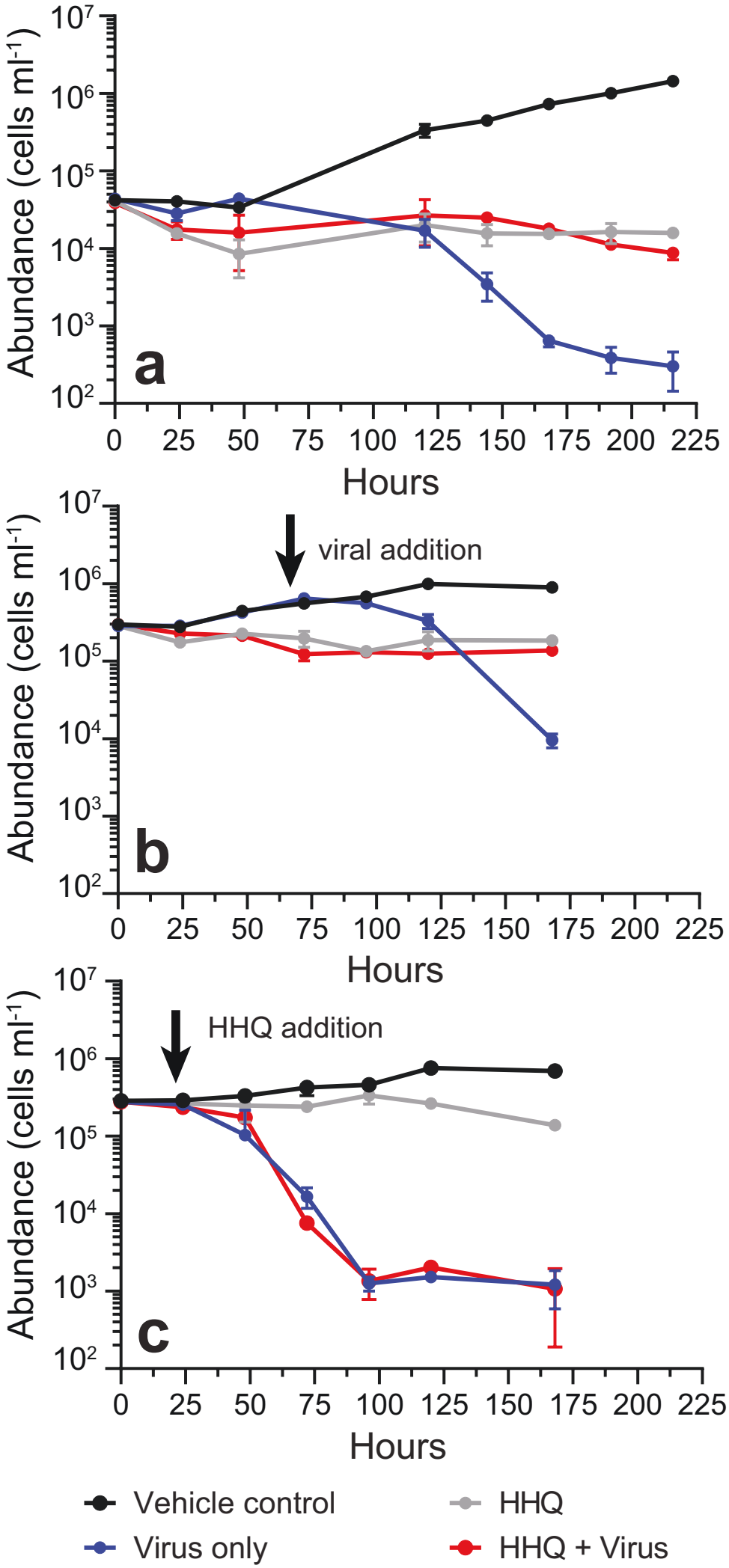
Abundance (cells ml-1)
10^7
10^6
10^5
10^4
10^3
10^2
a
0 25 50 75 100 125 150 175 200 225
Hours
viral addition
b
HHQ addition
c
Vehicle control
Virus only
HHQ
HHQ + Virus

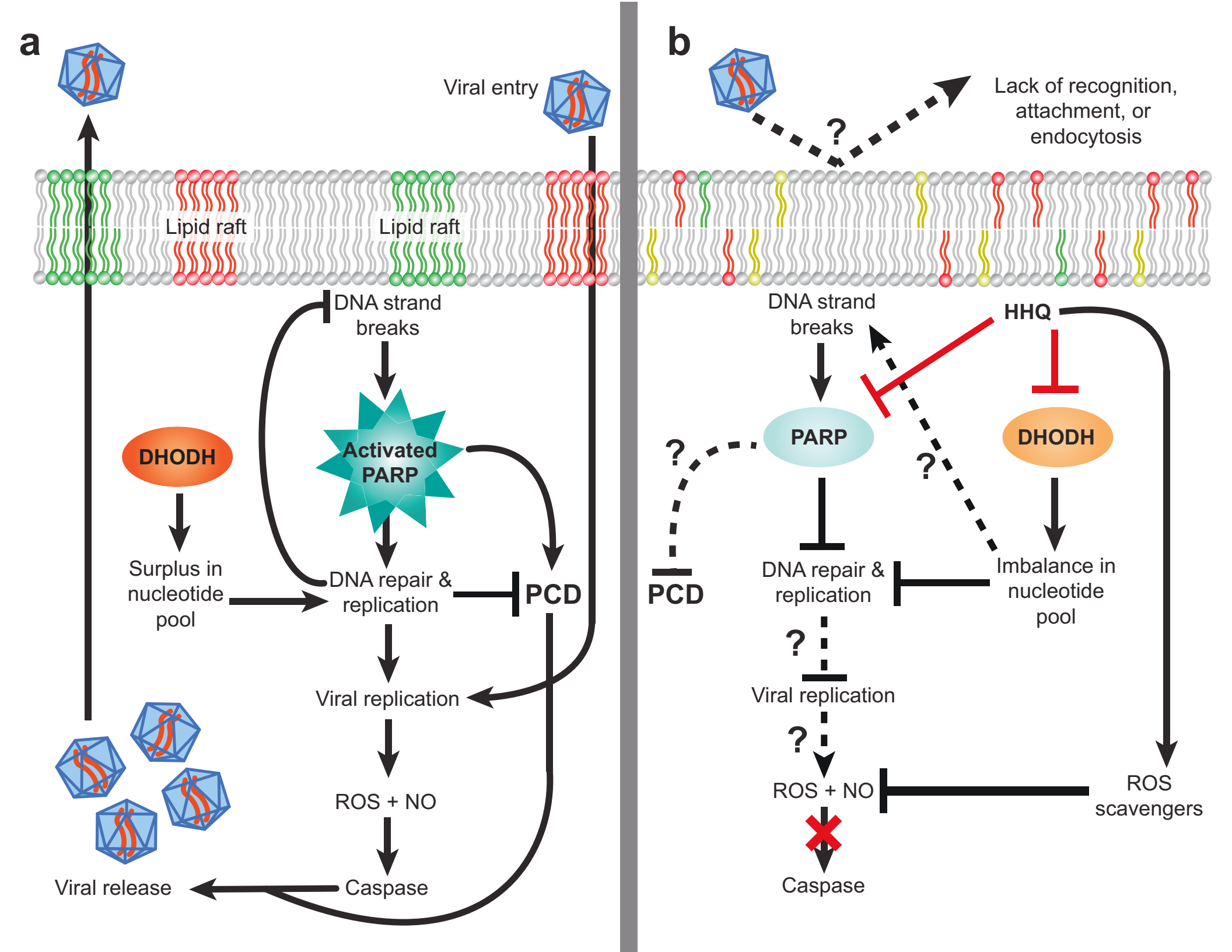
a
Viral entry
Lipid raft
Lipid raft
DNA strand breaks
DHODH
Activated PARP
Surplus in nucleotide pool
DNA repair & replication
PCD
Viral replication
ROS + NO
Caspase
Viral release
b
Lack of recognition, attachment, or endocytosis
DNA strand breaks
HHQ
PARP
DHODH
PCD
DNA repair & replication
Imbalance in nucleotide pool
Viral replication
ROS + NO
ROS scavengers
Caspase